Journal of Materials Chemistry C

Accepted Manuscript

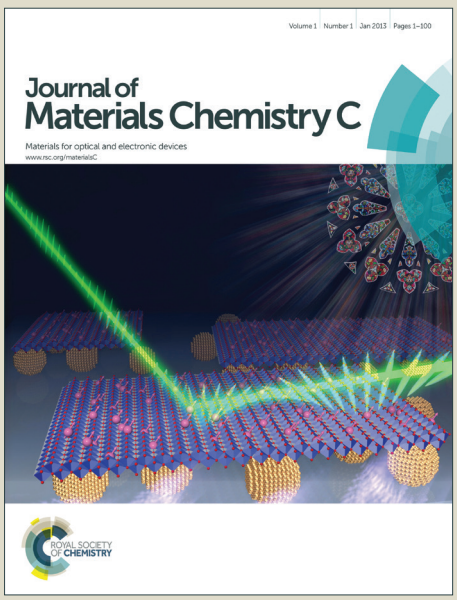

ROYAL SOCIETY OF CHEMISTRY

www.rsc.org/materialsC

Solution- and Solid-State Photophysical and Stimuli-Responsive Behavior in Conjugated Monoalkoxynaphthalene-Naphthalimide Donor-Acceptor Dyads

Cameron Peebles, Christopher D. Wight, and Brent L. Iverson*

Department of Chemistry, The University of Texas at Austin, Welch Hall 2.204, 105 E. 24th St. A5300, Austin, TX 78712 USA

ABSTRACT: The stimuli-responsive properties of a series of aromatic conjugated monoalkoxynaphthalene-naphthalimide donor-acceptor dyads were studied. Two of the dyads, dyads **1** and **4**, showed a difference in solid-state color between relatively faster (yellow) and slower (yellow-orange or orange) evaporation from solution, while the other dyads, dyad **2** and **3**, only showed one color (yellow-green) for both evaporation rates. Importantly, highly solvatochromic dyad **4** displayed thermochromic (orange to yellow), mechanochromic (orange to yellow) and vapochromic (yellow to orange) stimuli-responsive behavior in the solid-state with repeatable cycles of color changing. Structural and spectroscopic studies indicated that the stimuli-responsive behavior of dyad **4** is the result of a 180° molecular rotation wherein the thermodynamically more stable head-to-head stacked orange crystalline solid interconverts with a head-to-tail stacked soft-crystalline yellow mesophase. The thermochromic transition of **4** from a presumably more stable crystalline state (orange) to a metastable soft crystalline mesophase state (yellow) that persists at room temperature unless exposed to solvent vapor is particularly noteworthy.

INTRODUCTION

Strongly fluorescent, or luminescent, organic materials whose fluorescence can be finely-tuned show great potential for applications in light-emitting diodes (LEDs),[1] optoelectronic devices,[2-3] and sensing materials.[4-5] One approach attracting increased attention involves the development of molecules that show changes in their photophysical properties upon reversibly switching their solid-state morphology in response to an external stimulus. These materials are called stimuli-responsive and undergo morphological (molecular packing) changes as a result of (but not limited to) changes in temperature (thermochromic)[1-4,6-12], pH (acidchromic)[7,13], pressure (mechanochromic)[1-3,6-13] and vapor (vapochromic).[2,6-7,10-11,13] Currently, many of these materials show stimuli-responsive behavior towards only one type of external stimulus, thus new molecular systems responsive to multiple external stimuli are still noteworthy.[7-8,11]

Of the types of stimuli-responsive behavior, mechanochromic materials are still considered rare, but are attracting increased attention.[5] In contrast to "normal" mechanochromic materials, whose absorbance properties change with applied force (pressure/grinding), mechanochromic materials whose fluorescence properties change with applied force (mechanoluminescent or piezoluminescent materials) are even less common. Applications for these molecules range from mechano-sensors to security papers and damage-indicators. The energetics of mechanochromic materials is typically straightforward: the material state after having been ground or pressed is often associated with a meta-stable state that can be reverted back to the thermodynamic state with additional stimuli (heating, solvent fuming, etc.).[14-15]

Stimuli-responsive luminescent organic molecules have been reported in both crystalline[16-17] and liquid crystalline[5] systems. Variable luminescence between liquid crystal and crystalline phases has also been reported for π-conjugated materials containing asymmetric side chains.[18] Seki *et al.* reported a mechanically-induced single-crystal-to-single-crystal transformation in a material subsequently leading to a luminescent color change (from blue to green).[19]

Previous experimental results from our group and others have revealed that in polar solvent or the liquid crystalline state, 1,4,5,8-naphthalenetetracarboxylic diimide (NDI) prefers to stack in a face-centered, alternating fashion with isosteric aromatics bearing electron-donating groups such as 1,5-dialkoxynaphthalene (DAN). In the solid state, however, NDI prefers to self-stack in an off-set geometry even if DAN is present. For example, hydrophilic NDI-DAN oligomers exclusively adopt a face-centered, alternating NDI-DAN geometry in aqueous solution, that give rise to a deep red charge-transfer absorbance even though both DAN and NDI are colorless.[20] We have also reported an amphiphillic folding NDI-DAN oligomer that adopts an alternating NDI-DAN stacking geometry in aqueous solution, but then forms a highly ordered amyloid-like solid involving NDI offset self-stacking.[21-22] NDI self-stacking has been seen in a variety

of other self-assembling systems, most notably those of Parquette.[23-25] Taken together, these results indicate that in aqueous solution, face-centered alternating NDI-DAN is favored by dominant desolvation forces driving the hydrophobic aromatic faces out of solution and into a central stack. In line with the model set forth by Wheeler and Houk,[26] we believe that the preference for alternating NDI-DAN stacking is directed by favorable, through-space interactions between polarized moieties on the periphery of the aromatic units; the carbonyls of NDI and the phenolic O atoms of DAN. In the solid state, due to the requirement for close contact between molecules without the influence of desolvation, NDI self-stacking in an offset mode predominates. The offset geometry optimizes electrostatic attraction because the electron-deficient carbonyl carbon atom of one NDI unit is situated directly above the relatively electron-rich carbonyl oxygen atom of an adjacent NDI unit.

The bottom line is that there is a delicate balance between NDI stacking in an alternating, face-centered geometry with aromatics such as DAN under certain circumstances, and NDI self-stacking in an off-set geometry in others. For example, Reczek *et al.* demonstrated that derivatives of DAN and NDI monomers mixed in a 1:1 ratio formed mesophases over a range of temperatures that exhibited a dark red color indicative of alternating, face-centered NDI-DAN stacking.[27] Interestingly, for several derivatives, upon cooling from the mesophase the dark red color becomes pale yellow or even white due to unstacking of the DAN and NDI monomers into separate microdomains. These domains were shown to be composed of stacks of off-set NDI self-stacked monomers and herringbone-stacked DAN monomers.[28]

More recently, we reported the synthesis and polymorphism of a series of conjugated aromatic monoalkoxynaphthalene (MAN) and naphthalene imide (NI) donor-acceptor (D-A) dyads **1**-**4** (Fig. 1a).[29] Dyad **1** was found to form two distinct and differently colored crystal forms as a function of crystal growth time: a yellow head-to-tail (NI-MAN aromatic interaction) crystal with green emission after faster evaporation (**1f**, 1-2 days) from chloroform (Fig. 1b) and a yellow-orange head-to-head (NI-NI aromatic interaction) crystal with orange emission after slower evaporation (**1s**, more than 5 days) from 1:1:1 Toluene:MeOH:Ethyl Acetate (Fig. 1c).[29] Orange crystals of dyad **4,** referred to as **4s** from now on, produced upon slower evaporation (more than 10 days) from 1:1:1 DCM:MeOH:Acetone displayed an orange-red emission (Fig. 1f) and were also found to contain a head-to-head (NI-NI) stacking geometry similar to that seen in the yellow-orange **1s** crystal (Fig. 1d). Dyad **4** did not generate crystals suitable for single crystal X-ray analysis following faster evaporation from a variety of solvents, although a yellow solid with green emission (Fig. 1g), referred to as **4f** from now on, was reproducibly formed. Neither dyad **2** or **3** displayed evaporation rate dependent color changes, as all solids were yellow-green in color and displayed a green fluorescence (Fig. 1h). Unfortunately, neither **2** or **3** formed crystals suitable for single crystal X-ray analysis after repeated attempts using either faster or slower evaporation from a variety of solvents. However, based on powder XRD data, it was proposed that both **2** and **3** were stacked in a head-to-tail fashion in the solids that formed. Based on XRD patterns and modeling we proposed that **4f** is also packed in a head-to-tail fashion as shown in Fig. 1e (symmetry elements are highlighted).

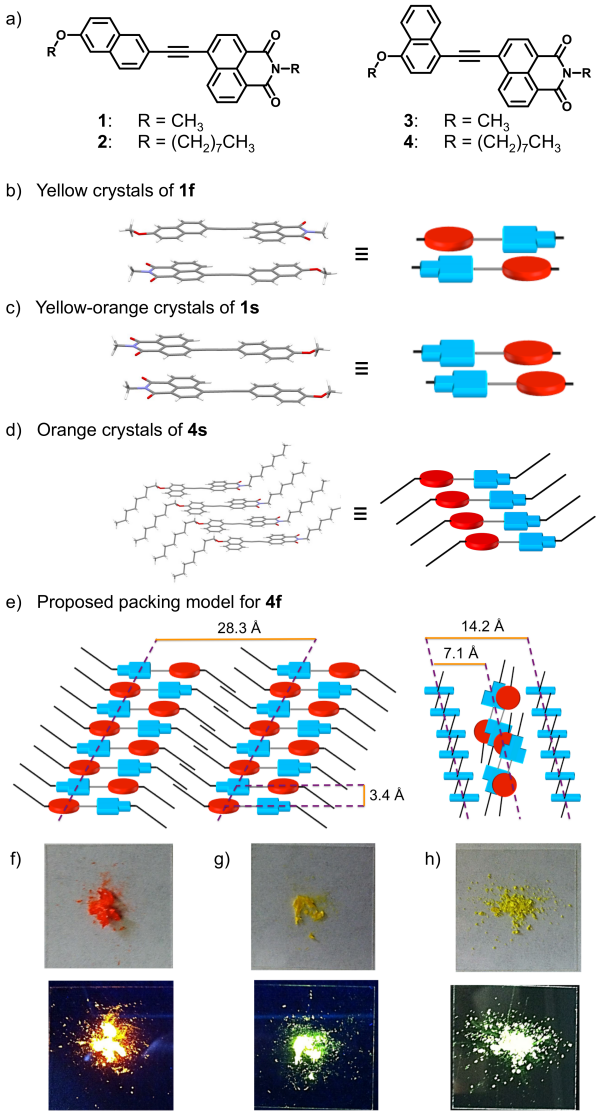

Fig. 1 Dyad structures, molecular packing based on single crystal X-ray analyses or modeling and representative yellow and orange solids. (a) Structures of **1** – **4**. (b) Crystal structure[29] and schematic packing of slower evaporated **1f** observed to stack in a head-to-tail orientation. (c) Crystal structure[29] and schematic packing of faster evaporated **1s** observed to stack in a head-to-head orientation. (d) Crystal structure[29] and schematic packing of slower evaporated **4s** observed to stack in head-to-head orientation. In the cartoons, the naphthalimide portion of the dyad is shown in blue and the monoalkoxynaphthalene portion in red. e) The proposed head-to-tail packing of **4f** as determined by XRD analysis and modeling. (f) **4s** orange solid with red emission. (g) Yellow solid with green emission formed from dyad **4f**. (h) **2** yellow solid with green emission.

During our investigation of the photophysical properties of dyads **1** - **4**, dyad **4** was discovered to exhibit extensive stimuli-responsive behavior when exposed to heat, pressure and solvent vapor. Herein is reported a series of studies of dyad **4** that describe this behavior in detail. A structural model is proposed in which the thermodynamically more stable head-to-head (NI-NI) stacked orange crystalline solid interconverts with a head-to-tail (NI-MAN) stacked soft crystalline meta-stable yellow mesophase.

EXPERIMENTAL SECTION

Detailed procedures for the synthesis of dyads **1** – **4** were previously reported.[29] Absorption spectra were taken on an Agilent 8453 UV-Vis spectrometer (50 μM concentrations for solution-state measurements). Fluorescence spectroscopy was performed on a PTI fluorimeter (100 nM concentrations for solution-state, 0.5 mm slits for solution-state, 2.00 mm slits for solid-state) equipped with a 814 photomultiplier detection system using a 75W xenon short arc lamp. Differential scanning calorimetry (DSC) was performed on a DSC Q100 from TA Instruments Waters (USA) at a scan rate of 5 °C/min under a Nitrogen air flow. Thermal gravitational analysis (TGA) was performed on a TA Instruments-Waters LLC TGA Q500 instrument. Powder X-ray diffraction (XRD) was obtained using a Scintag X1 theta-theta diffractometer equipped with a Cu X-ray tube and solid-state X-ray detector set to count Cu Kα radiation. X-ray crystallography was performed on a Nonius Kappa CCD diffractometer using a Bruker AXS Apex II detector and a graphite monochromator with Mo Kα radiation (λ = 0.71075 Å). Specific details for the collection and analysis of the **4s** crystal were previously reported.[29]

RESULTS AND DISCUSSION

Solvatochromic Properties. A strong bathochromic shift in emission (spanning 135 nm) was observed upon dissolving **4** in solvents of varying polarity (see Fig. 2). A more comprehensive discussion of the photophysical properties of **4** can be found in the Supporting Information. The positive solvatochromism of the emission can be seen by the naked eye with **4** exhibiting a blue fluorescence in *n*-hexane (λ_{max}, 444 nm), but a yellow/orange fluorescence in acetone (λ_{max}, 579 nm). Quantum fluorescence yields (Φf) were calculated using the comparative method and details of this experiment can be found in the Supporting Information. A broad absorption band was present for each solvent and the absorption maximum was seen to undergo a bathochromic shift upon changing from *n*-hexane (403 nm) to acetone (419 nm). Ground state (μgD) and excited state (μeD) dipole moments of **4** were calculated by generating a Lippert-Mataga plot. An explanation of the Lippert-Magata equation and how the dipole moments were generated can be found in the Supporting Information. In agreement with the observed solvatochromism, our calculations showed dyad **4** to have an overall dipole change of 47.5 D upon going from the ground to excited state. Concentration dependent emission fluorescence measurements were performed (see the Supporting Information) to verify that the mode of electron transfer in the dyad excited states was due to an intramolecular photoinduced-electon transfer (PET) process rather than a Förster resonance energy transfer (FRET) process.

Fig. 2 Positive solvatochromism displayed by **4** upon increasing solvent polarity under UV irradiation (from left to right: *n*-hexanes, toluene, EtOAc, THF, DCM, acetone.)

Thermochromic Properties. Upon heating crystals of **4s** at 110°C for 30 seconds, an obvious and dramatic color change from orange to yellow occurred while remaining in a solid phase (Fig. 3). Importantly, the yellow form did not revert back to the initial orange color for the duration of the study (12 months when stored at room temperature).

In multiple examples, the thermochromic change from orange to yellow was observed to begin on the edge of the orange crystal, working its way inward, then end towards the middle. Heating does not change the macroscopic morphology of the original crystal, indicating that reorganization of the dyad packing is occurring at a microdomain level only.[27-28]

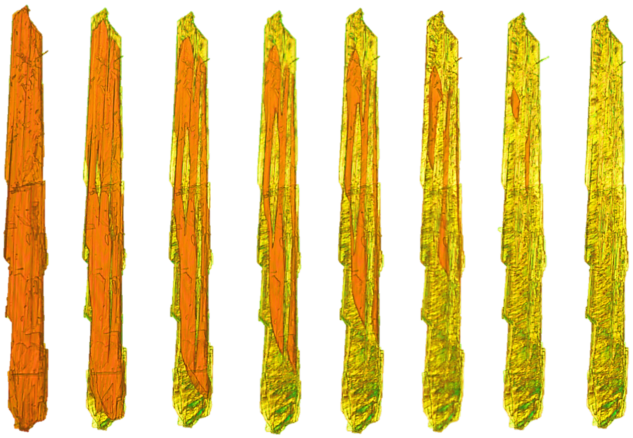

Fig. 3 Photographs of the thermochromic behavior of **4s**. Optical microscope images of heating **4s** at 110 °C showing the conversion to a yellow form after 30 seconds without any change in macroscopic morphology of the crystal.

Mechanochromic and Vapochromic Properties. Upon taking a sample of **4s** and grinding it with a pestle, the orange solid turned yellow indicating that the material is mechanochromic (mechanoluminescent) in nature. As shown in Fig. 4a, the initials for The University of Texas at Austin "UT" were ground into a glass plate covered with orange **4s** thus making the initials yellow.

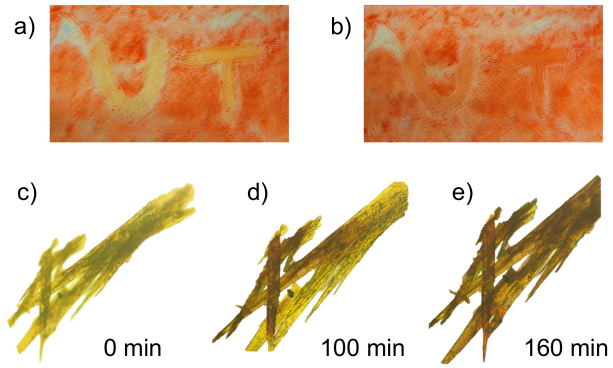

Fig. 4 Mechanochromic and vapochromic behavior of **4**. (a) The initials "UT" appear in yellow after grinding with a glass rod a glass plate coated in **4s**. (b) Vapor-fuming of the glass plate shown in (a) reverts the yellow "UT" initials back to orange. (c) – (e) Crystals of **4s** were placed on a glass slide and heated at 110 °C and converted to the yellow form. The yellow solid was transferred to a vapor-fuming chamber containing DCM. The glass slide was transferred between the optical microscope and the fuming chamber to collect images of the transformation every 20 minutes. Images captured at time equals 0, 100 and 180 minutes are presented.

Subjecting the glass plate on which "UT" had been mechanically ground to vapor-fuming with DCM reverted the yellow "UT" letters back to orange (Fig. 4b). Similarly, subjecting a sample of either the yellow solid formed after grinding **4s**, or the yellow solid formed after heating **4s,** to vapor-fuming with a 1:1:1 mixture of DCM:MeOH:Acetone at room temperature and ambient pressure yielded orange crystals (or solid in the case of the ground material) after a period of 1 day (overnight). Vapor-fuming of quickly formed solid **4f** with 100% DCM also gave a color change to orange crystals over the course of 1 day (Fig. 4c-e), however, vapor-fuming with *n*-hexane and MeOH over 1 week did not have any effect on the color of the crystals (stayed yellow). Interestingly, while vapor-fuming **4f** on a bulk scale produced an orange-colored looking material (Fig. 4b), vapor-fuming on a single crystal level returned a more red-colored looking material (Fig. 4e) (see Supporting Information Fig. S3 for more images of the single crystal vapor-fuming process).

Shearing and Texture Properties. When a single crystal of the initially evaporated yellow **4f** is sandwiched between two glass slides and a shear force applied the crystal material smeared (Fig. 5a). As seen in Fig. 5b, when the same shearing force was applied to crystals of **4s** the crystals broke into smaller shards retaining their crystalline form. This result suggested that **4f** was not in the crystalline state and further investigation into the yellow material phase was pursued.

Upon drop-casting a solution of **4** from DCM onto a glass slide (leaving a yellow solid after rapid evaporation) and looking at the solid under cross-polarized light using a polarized OM (POM) spherulite-like textures were observed (Fig. 6a).

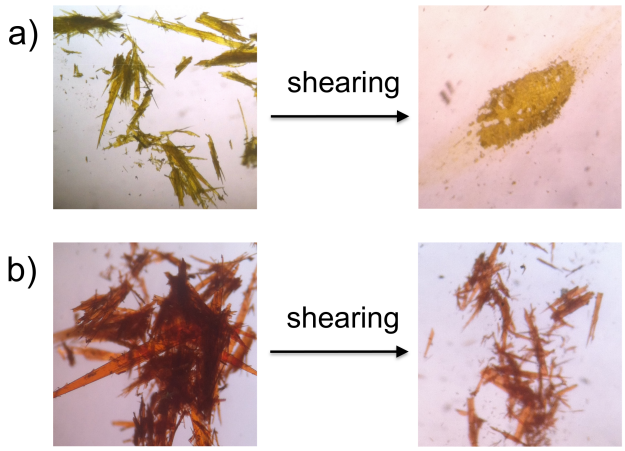

Fig. 5 Photographs of shearing effects on (a) **4f** and (b) **4s**. While **4f** smears, **4s** remains crystalline.

With this result in mind, crystals of **4s** were heated on a hot plate past their melting point (~130 °C), allowed to sit at 150 °C for 5 minutes, and then slowly cooled at a rate of 5 °C per minute to room temperature. Investigation of the resulting yellow material under cross-polarized POM revealed spherulite-like textures similar to those shown by drop-casting a solution of **4** at room temperature (Fig. 6b).

Liquid Crystalline Mesophase Properties. Further investigation of the crystallization process of **4** was carried out using a POM. To this end, solid **4s** was placed on a microscope slide and subsequently placed on a hot stage attached to the POM and heated to its melt. The sample was then cooled at a rate of 5 °C/min and the crystallization process observed. Surprisingly, at ~ 125 °C, fan-like liquid crystal textures emerged that were characteristic of a Smectic A (SmA) liquid crystalline mesophase (Fig. 6c). This texture remained until the material was cooled to 115 °C, at which point the SmA texture disappeared.

Thermal Analysis. Thermal analysis using DSC of **4f** showed a large endothermic transition at 133.68 °C (14.85 kJ/mol) corresponding to the melting point of the dyad (Fig. 7a). The DSC heating trace for **4s**, however, showed a smaller broad endothermic peak at 98.39 °C (38.8 kJ/mol) as well as a larger endothermic peak at 132.49 °C (19.5 kJ/mol). Both of these DSC traces can be repeated using the non-crystalline solid material for both the relatively faster and slower evaporated species with the same results in the DSC analysis. The smaller endothermic peak

at 98.39 °C is strongly indicative of a phase transition[3,6-7,9,12-13].

The yellow solid generated by heating **4s** was subjected to XRD and the obtained patterns were near identical to those of **4f** generated directly by faster evaporation (Fig. 7a). In agreement with the images of the thermally driven orange to yellow conversion and the DSC trace, this strongly indicates that heating crystalline **4s** gives the soft crystalline mesophase **4f**.

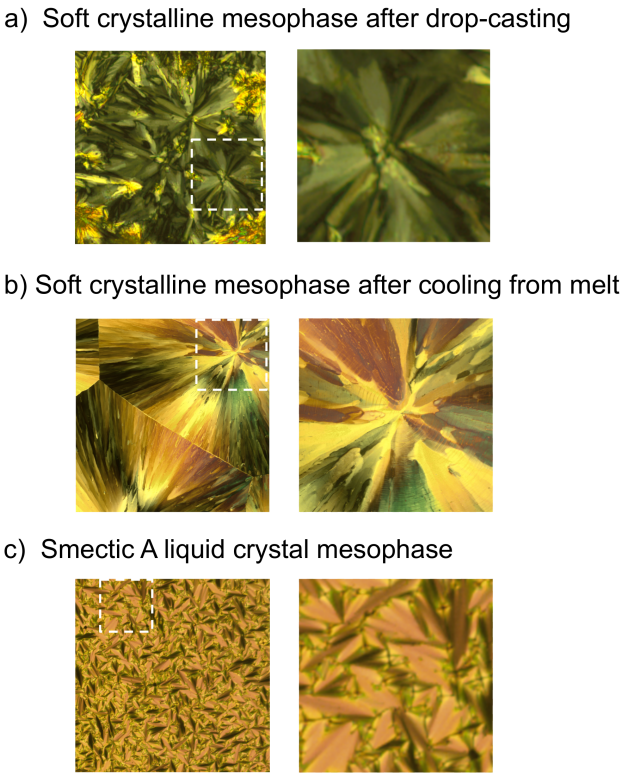

Fig. 6 Representative POM images of the soft crystalline and liquid crystalline mesophases of **4**. (a) Soft crystalline mesophase of **4f** after drop-casting on a glass slide at room temperature; (b) Soft crystalline mesophase of **4f** after having been slowly cooled from the isotropic state; (c) Fan-like Smectic A textures in the liquid crystalline mesophase state of **4** at an elevated temperature. Images on the right are blown-up sections of the white dashed boxes on the left images.

In addition to DSC measurements, thermal gravimetric analysis (TGA) was conducted to verify that the phase transition of **4s** to **4f** at ~100 °C was the result of only molecular rearrangement of the dyads and not by loss of solvent from the crystal matrix. Supporting Information Fig. S4 shows the overlap of TGA and DSC curves for heating **4s** under the same experimental conditions (thermal ramp of 5 °C/min). While heating from 90 to 110 °C, where the solid phase transition occurs, there was a weight loss of 0.08435% which is comparable to the weight loss observed upon melting from 130 °C to 150 °C (0.09800%) on the same TGA experiment. As mentioned earlier, the crystal structure of **4s** did not show any solvent molecules in its crystal lattice. Taken together, these data indicate that the thermal transition from **4s** to **4f** is not due to removal of solvent from the crystal lattice, but instead rearrangement of dyad molecular packing.

The vapor-fuming generated orange solid was analyzed in a number of ways. Optical spectroscopy revealed an

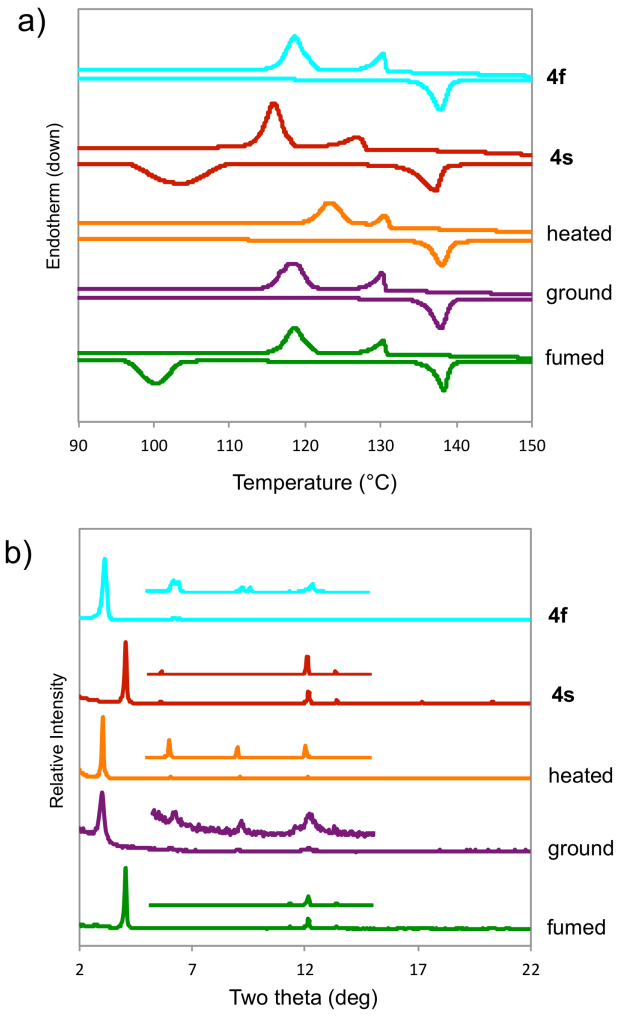

Fig. 7 (a) DSC traces (scan rate of 5 °C / min) and (b) powder XRD patterns for **4f**, **4s** and when external stimuli are applied.

absorbance maximum (536 nm) and fluorescence maximum (574 nm) that match those of **4s** (542 and 576 nm, respectively). Thermal analysis of the vapor-fuming generated orange solid looked very similar to that of the slower evaporated **4s** and yielded a broad endothermic peak at 98.39°C (45.07 kJ/mol) and a sharp endothermic peak at 134.35 °C (25.58 kJ/mol) representative of a phase transition and the melting point, respectively (Fig. 7a).[3,6-7,9,12-13] Two recrystallization exothermic peaks were also present at 130.21 °C (5.89 kJ/mol) and 122.26 °C (18.37 kJ/mol). Subjecting the vapor-fuming generated orange solid to XRD analysis gave a crystalline pattern that exactly matches that of the **4s** pattern (Fig. 7b).

The back and forth conversion process of orange to yellow and yellow to orange appears to be entirely reversible. Fig. 8 shows the maximum emission of the solid after repeated cycles of heating and vapor-fuming and indicate that this material can undergo multiple heating-fuming cycles without significant change to the emission spectra of either state.

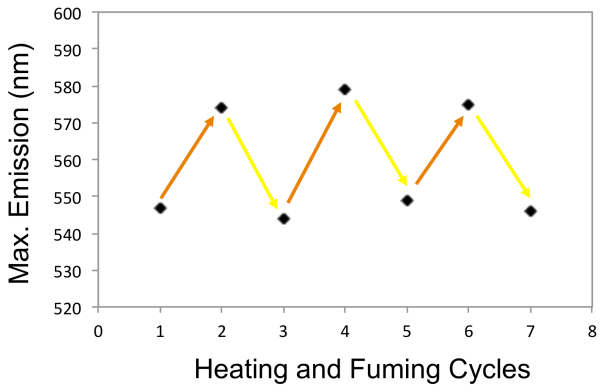

Fig. 8 Repetitive cycles of heating and fuming **4** consistently give nearly the same emission maximum for **4f** (545 nm) and **4s** (576 nm).

Taken together, these data are entirely consistent with the hypothesis that crystalline orange **4s** is regenerated from the yellow **4f** by vapor-fuming. Importantly, the fuming process uses the same solvent system (1:1:1 DCM:MeOH:Acetone) as is initially used to generate crystals of **4s** suitable for single crystal X-ray analysis. Recall that no solvent molecules are seen in the X-ray analysis of **4s**, thus it seems likely that vapor-fuming **4f** back to **4s** is not the result of introducing solvent molecules into the solid. Additionally, repetitive cycles of heating and vapor-fuming **4** gave nearly the same emission maximum as the initially quickly (545 nm) and slowly (576 nm) evaporated **4f** and **4s.**

As expected, heating **4s** to the isotropic state with subsequent cooling (5 °C/min) yielded two exothermic crystallization peaks at 126.84 °C (4.29 kJ/mol) and 119.03 °C (15.94 kJ/mol) with the resulting solid material being yellow (Fig. 7a). Repeating the heating of **4s** using DSC with sequential slow cooling (1 °C/min from 160 °C down to 40 °C) again lead to the formation of **4f** with the same exothermic crystallization peaks occurring. The first crystallization event of **4f** (the Iso-SmA transition) displays a transition energy of ~5 kJ/mol which matches those of previously reported Iso-SmA transition energies. The second crystallization event (SmA-soft crystalline mesophase) has a transition energy of ~16 kJ/mol which is smaller than both the **4s**-**4f** (38.8 kJ/mol) and **4f**–Iso (19.5 kJ/mol) phase transitions. Powder XRD of this material matched that of both the initially formed yellow solid **4f** and the heated and ground yellow solids (Supporting Information Fig. S5) indicating the structural morphology of the three solids is the same. The previously detailed drop-cast experiments demonstrated that the soft crystalline mesophase observed upon cooling **4** from the liquid crystalline mesophase to the soft crystalline mesophase did not retain the LC textures due to quenching effects. Importantly, this observation revealed that between ~125-115 °C the yellow polymorph **4f** is in a liquid crystal mesophase. Upon cooling below ~115 °C **4f** undergoes a transition to a soft crystalline mesophase.

DISCUSSION

Previously, we had shown that compounds **1** and **4** form two distinct solids as a function of solvent and solvent evaporation time.[29] Slower evaporation yielded yellow-orange and orange **1s** and **4s**, respectively, while faster evaporation gave yellow **1f** and **4f**. Compounds **2** and **3** gave only yellow-green solids regardless of evaporation time or solvent used. Solids **1f**, **1s** and **4s** were found to be crystalline. Single crystal X-ray analysis revealed a head-to-head (NI-NI interaction) stacking geometry (See Fig. 1d) for both **1s** and **4s**. On the other hand, the structure of yellow **1f** revealed a head-to-tail (NI-MAN interaction) geometry. Based on powder XRD analysis and detailed modeling we conclude that **4f** is also stacked in a head-to-tail (NI-MAN) geometry. Therefore, based on structural similarity to **1s** and **1f**, we assume that interconversion of **4s** and **4f** involves a 180° rotation motion that is normal to the long axis of the molecules. Because **4f** is a soft crystalline mesophase while **4s** is crystalline, interconversion of the two also leads to a change in the dynamic mobility of the molecules after the interconversion. Nevertheless, it appears that both forms have at least similar packing densities as the gross macroscopic crystal dimensions and morphology do not change significantly upon heating a crystal of **4s** to give **4f** (Fig. 3). We are currently attempting to obtain more quantitative data with respect to any small volume changes that may accompany the **4s** to **4f** transition.

Both stacking geometries of **4** have strong precedent with similar imide or diimide molecules. Recent computational work by Wheeler[30] and Wheeler *et al.*[31] have put forth an explanation of aromatic stacking interactions in which local, direct through-space interactions between polarized moieties on the periphery of stacked aromatic units drive the aromatic stacking geometry. Consistent with these predictions,[27-28] NDI-NDI and by analogy NI-NI stacking in the crystalline state can be understood as having electrostatic interactions dominated by the highly polarized carbon-oxygen bonds of diimide and imide units. In particular, as seen in **4s**, the head-to-head offset self-stacking mode positions the electron-rich carbonyl oxygen atom of one dyad directly above the relatively electron-deficient outer edge of the NI aromatic core of an adjacent imide molecule unit. Conversely, the proposed head-to-tail NI-MAN stacking in the yellow soft crystalline mesophase **4f** resembles the alternating face-centered stack we have previously observed in soft/plastic liquid crystal mesophases of DAN and NDI monomers.[27-28] We assume these alternating **4f** stacks are dictated by

interactions between the electron-rich ether O atom of a MAN unit interacting with electron-deficient areas of an adjacent NI, most likely the carbonyl carbon atom.

The different absorbance and emission wavelengths seen in **4f** and **4s** can be attributed to at least two possible causes. First, based on analogy to the yellow **1f** and yellow-orange **1s** for which crystal structures are known, it is reasonable to propose that head-to-tail stacking of **4f** leads to an electronic environment that dictates shorter wavelength absorption and emission, while the head-to-head stacking of **4s** leads to an electronic environment that dictates longer wavelength absorbance and emission.[32] Second, for the sake of completeness, we cannot formally rule out the possibility that there is a different amount of twisting of the two aromatic units with respect to each other in **4f** vs. **4s**. The aromatic units are coplanar in the crystal structure of the orange **4s**, yellow **1f**, and orange **1s**, but we have no information with regard to twisting in **4f**. Our DFT calculations (Supporting Information Fig. S6) predict longer wavelength absorbances and emissions in the case of highly twisted dyad structures, so a twisted structure in **4f** could in theory contribute to its photophysical properties although there is no evidence to support such a hypothesis.

The presence of two forms of **4** that can be interconverted in the solid state raises interesting thermodynamic questions. From the evaporation time-dependent formation of the two forms, it is intuitive to suggest that since **4s** takes longer to form relative to **4f** (10 days versus 1 day, respectively), **4s** is the thermodynamically more stable state. This assumption is in agreement with Ostwald's step rule.[33] A similar view of evaporation-dependent kinetics has been proposed in other systems displaying polymorphic and stimuli-responsive behavior.[19,34] Upon heating **4f** to its melt and allowing it to cool at a rate of 5 °C/min, a liquid crystalline mesophase was observed by DSC and POM between ~ 125-115 °C while a soft crystalline mesophase was observed by POM upon cooling to room temperature. Powder XRD of the room temperature soft crystalline mesophase material matched that of yellow samples generated using other methods (**4** quickly evaporated from solvent, **4s** crystals heated without melting, or ground **4s**), so we assume that all of these yellow samples of **4f** are similarly a soft crystalline mesophase. The picture that emerges is one in which the yellow soft crystalline mesophase **4f** is formed faster than **4s** upon solvent evaporation, yet once formed, **4f** is kinetically trapped in the less stable state at or around room temperature.

Conversion of **4s** to the soft crystalline mesophase **4f** upon grinding appears to be in line with the behavior of several previously reported materials. In particular, it has been observed that grinding a crystalline state of a mechanochromic material generally leads to a metastable and more amorphous state.[7,9-10,12-13]

The conversion of **4f** to **4s** in the presence of vapor from certain solvents over a 24-hour period is also consistent with previously reported vapochromic systems. In particular, it has generally been observed that exposure to solvent vapor leads to the conversion of a metastable state to a more stable state[7] and/or conversion of a more amorphous state to a more crystalline state.[2,8,10-11,35] Recall that TGA and single crystal experiments revealed that there are no solvent molecules present in the crystal lattice of **4s**. Therefore, we assume the solvent molecules are only playing a transient role in the crystallization process from the soft crystalline mesophase state of **4f**. A reasonable hypothesis is that the solvent molecules from vapor temporarily diffuse at least some extent into the solid and are able to provide a sufficient level of mobility to allow for the slow rearrangement necessary to produce **4s**.

In contrast to the observed mechanochromic and vapochromic behaviors, the thermochromic behavior of **4s** is counterintuitive and to the best of our knowledge unique among stimuli-responsive materials. One would ordinarily expect heating of a thermochromic solid to facilitate the conversion of a metastable and higher energy form, especially one that is a soft crystalline mesophase such as **4f**, to a presumably lower energy form such as **4s**, not the reverse as was observed in our study. Indeed, other thermochromic materials generally display a change from a less ordered state to more ordered state[2,13,35-36] or a metastable state to lower energy state upon heating.[1,7,9,12] It is not clear why heating the presumably lower energy crystalline form of **4s**, while staying well below its melting temperature, would lead to the apparent complete conversion to a higher energy form, **4f**, especially considering a dramatic 180° reorientation required of at least half the molecules in the solid (documented in Fig. 3). Since both **4s** and **4f** have long-range order, the only conclusion to draw thus far is that there appears to be some structural link between the presence of dynamic motion and enhanced stability of head-to-tail stacking in **4f**. The exact nature of that link is currently not known.

In previously reported work, a molecular "domino" effect was proposed to describe a mechanically-driven phase transition between two polymorphs.[19] In the present research, the thermally-driven **4s** to **4f** transition was observed to occur along the edges of single crystals and propagate inwards (see Fig. 3). It is therefore reasonable to suggest a similar domino effect in the conversion of **4s** to **4f.** In particular, it can be proposed that relative to interior molecules, the molecules along the edge of the **4s** crystal lattice have more molecular freedom. Edge molecules could therefore be expected to reorient first as the result of higher temperature or mechanical pressure, leading to molecular rearrangements that propogate inward through the crystal. An alternative mechanism whereby all molecules shift simultaneously (leading to a sudden color change across the entirety of the crystal) was not observed upon heating, perhaps due to the high energy cost for such a sudden and dramatic reorientation.

CONCLUSIONS

In summary, we have demonstrated the stimuli responsive behavior of a NI-MAN conjugated dyad **4** in which

the photophysical properties of the dyad can be switched by heating, grinding and vapor-fuming. Based on single crystal data, XRD patterns and modeling we propose the change in the dyad color upon external stimuli is based on a 180° rotation relative to the long axis of the molecule. A number of other key questions remain concerning the stimuli-responsive behavior of **4**. For example, it is not clear why the head-to-tail assembly seen in **1f** and **4f** forms faster relative to head-to-head stacking seen in **1s** and **4s**. Further, it is unclear why **4f**, despite being a soft crystalline mesophase, is prevented from returning to the apparently lower energy **4s** crystalline even after extended periods at room temperature (12 months). Future studies will continue to probe these questions and other details of the interesting stimuli-responsive behavior of **4** and its analogs.

ASSOCIATED CONTENT

Supporting Information

Quantum fluorescent yields, Lippert-Magata calculations, fluorescence concentration plots, TGA data, melting XRD and DFT calculations. This material is available free of charge via the Internet at http://pubs.acs.org.

AUTHOR INFORMATION

Corresponding Author

* (B.L.I.) E-mail: iversonb@austin.utexas.edu.

Notes

The authors declare no competing financial interest.

ACKNOWLEDGMENTS

This work was supported by the Robert A. Welch Foundation, grant F1188 to B.L.I. We would like the thank Dr. Eric Anslyn and his group for use of their fluorimeter, Dr. C. Grant Willson and his group for use of their DSC, Dr. Chris Bielawski and his group for use of their TGA, Dr. Jonathan Sessler and his group for use of their POM, and Dr. Steve Swinnea for collecting XRD data.

ABBREVIATIONS

LEDs, light-emitting diodes; NDI, 1,4,5,8-Naphthalenetetracarboxylic diimide; DAN, 1,5-Dialkoxynaphthalene; MAN, Monoalkoxynaphthalene; NI, Naphthalene imide; D-A, Donor-acceptor; DCM, Dichloromethane; MeOH, Methanol; XRD, X-ray diffraction; DSC, Differential Scanning Calorimetry; TGA, Thermal gravitational analysis; PET, Photoninduced-electron transfer; FRET, Förster resonance energy transfer; OM, Optical microscope; POM, Polarized optical microscope; CCD, Charge-coupled device; DFT, Density functional theory.

REFERENCES

(1) Gu, X.; Yao, J.; Zhang, G.; Yan, Y.; Zhang, C.; Peng, Q.; Liao, Q.; Wu, Y.; Xu, Z.; Zhao, Y.; Fu, H.; Zhang, D. *Adv. Funct. Mater.* **2012**, *22*, 4862.

(2) Gong, Y.; Tan, Y.; Liu, J.; Lu, P.; Feng, C.; Yuan, W. Y.; Lu, W.; Sun, J. Z.; He, G.; Zhang, Y. *Chem. Commun.* **2013**, *49*, 4009.

(3) Wang, L.; Wang, K.; Zou, B.; Ye, K.; Zhang, H.; Wang, Y. *Adv. Mater.* **2015**, *27*, 2818.

(4) Lumb, I.; Hundal, M. S.; Corbella, M.; Gómez, V.; Hundal, G. *Eur. J. Inorg. Chem.* **2013**, *27*, 4799.

(5) Sagara, Y.; Kato, T. *Nat. Chem.* **2009**, *1*, 605-610.

(6) Luo, W.; Zhao, W.; Shi, J.; Li, C.; Liu, Z.; Bo, Z.; Dong, Y. Q.; Tang, B. Z. *J. Phys. Chem. C* **2012**, *116*, 21967.

(7) Dou, C.; Han, L.; Zhao, S.; Zhang, H.; Wang, Y. *J. Phys. Chem. Lett.* **2011**, *2*, 666.

(8) Shan, X.-C.; Zhang, H.-B.; Chen, L.; Wu, M.-Y.; Jiang, F.-L.; Hong, M.-C. *Cryst. Growth Des.* **2013**, *13*, 1377.

(9) Tsukuda, T.; Kawase, M.; Dairiki, A.; Matsumoto, K.; Tsubomura, T. *Chem. Commun.* **2010**, *46*, 1905.

(10) Rao, S. M.; Liao, C.-W.; Su, W.-L.; Sun, S.-S. *J. Mater. Chem. C* **2013**, *1*, 5491.

(11) Shan, X.-C.; Jiang, F.-J.; Chen, L.; Wu, M.-Y.; Pan, J.; Wan, X.-Y.; Hong, M.-C. *J. Mater. Chem. C* **2013**, *1*, 4339.

(12) Zhang, Z.; Yao, D.; Zhou, T.; Zhang, H.; Wang, Y. *Chem. Commun.* **2011**, *47*, 7782.

(13) Rao, S. M.; Liao, C.-W.; Su, W.-L.; Sun, S.-S. *J. Mater. Chem. C* **2013**, *1*, 6386.

(14) Urban, M. W. Handbook of Stimuli-Responsive Materials; Wiley-VCH, 2011.

(15) Shan, G.-G.; Li, H.-B.; Cao, H.-T.; Sun, H.-Z.; Zhu, D.-X.; Su, Z.-M. *Dyes Pigments* **2013**, *99*, 1082.

(16) Sagara, Y.; Mutai, T.; Yoshikawa, I.; Araki, K. *J. Am. Chem. Soc.* **2007**, *129*, 1520.

(17) Kunzelman, J.; Kinami, M.; Crenshaw, B. R.; Protasiewicz, J. D.; Weder, C. *Adv. Mater.* **2008**, *20*, 119.

(18) Yagai, S.; Okamura, S.; Nakano, Y.; Yamauchi, M.; Kishikawa, K.; Karatsu, T.; Kitamura, A.; Ueno, A.; Kuzuhara, D.; Yamada, H.; Seki, T.; Ito, H. *Nat. Commun.* **2014**, *5*, doi:10.1038/ncomms5013.

(19) Ito, H.; Muromoto, M.; Kurenuma, S.; Ishizaka, S.; Kitamura, N.; Sato, H.; Seki, T. *Nat. Commun.* **2013**, *4*, doi: 10.1038/ncomms3009.

(20) Gabriel, G. J.; Iverson, B. L. *J. Am. Chem. Soc.* **2002**, *124*, 15174.

(21) Peebles, C.; Piland, R.; Iverson, B. L. *Chem. Eur. J.* **2013**, *19*, 11598.

(22) Bradford, V. J.; Iverson, B. L. *J. Am. Chem. Soc.* **2008**, *130*, 1517.

(23) Shao, H.; Parquette, J. R. *Angew. Chem. Int. Ed.* **2009**, *48*, 2525.

(24) Shao, H.; Nguyen, T.; Romano, N. C.; Modarelli, D. A.; Parquette, J. R. *J. Am. Chem. Soc.* **2009**, *131*, 16374.

(25) Shao, H.; Seifert, J.; Romano, N. C.; Gao, M.; Helmus, J. J.; Jaroniec, C. P.; Modarelli, D. A.; Parquette, J. R. *Angew. Chem. Int. Ed.* **2010**, *49*, 7688.

(26) Wheeler, S. E.; Houk, K. N. *J. Am. Chem. Soc.* **2008**, *130*, 10854.

(27) Reczek, J. J.; Villazor, K. R.; Lynch, V.; Swager, T. M.; Iverson, B. L. *J. Am. Chem. Soc.* **2006**, *128*, 7995.

(28) Alvey, P. M.; Reczek, J. J.; Lynch, V.; Iverson, B. L. *J. Org. Chem.* **2010**, *75*, 7682.
(29) Peebles, C.; Alvey, P. M.; Lynch, V.; Iverson, B. L. *Cryst. Growth Des.* **2014**, *14*, 290.
(30) Wheeler, S. E. *J. Am. Chem. Soc.* **2011**, *133*, 10262.
(31) Wheeler, S. E.; McNeil, A. J.; Müller, P.; Swager, T. M.; Houk, K. N. *J. Am. Chem. Soc.* **2010**, *132*, 3304.
(32) Zhang, X.; Chi, Z.; Zhang, Y.; Liu, S.; Xu, J. *J. Mater. Chem. C* **2013**, *1*, 3376.
(33) Threlfall, T. *Org. Process Res. Dev.* **2003**, *7*, 1017.
(34) Lee, A. Y.; Lee, I. S.; Myerson, A. S. *Chem. Eng. Technol.* **2006**, *29*, 281.
(35) Lou, X.; Zhao, W.; Shi, J.; Li, C.; Liu, Z.; Bo, Z.; Dong, Y. Q.; Tang, B. Z. *J. Phys. Chem. C* **2012**, *116*, 21967.
(36) Ooyama, Y.; Harima, Y. *J. Mater. Chem.* **2011**, *21*, 8372.

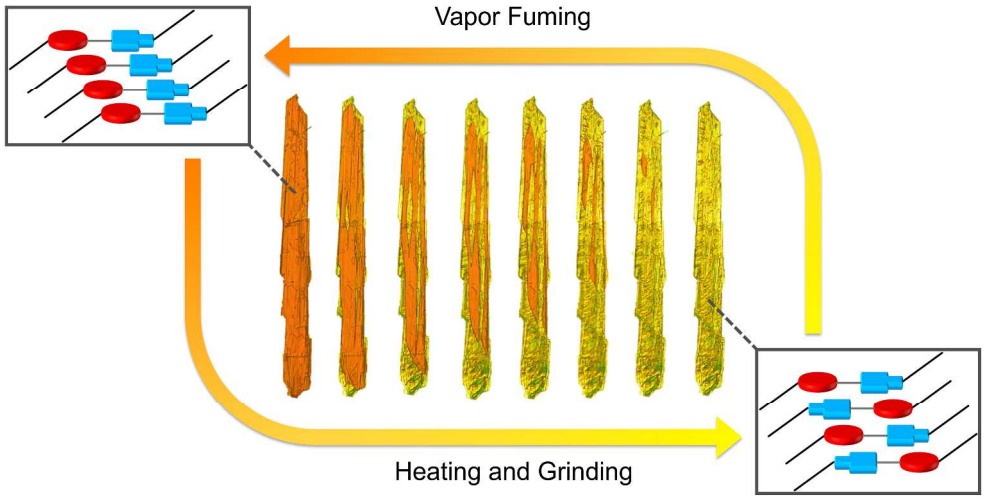

The solution-state, solid-state and exceptional stimuli-responsive properties of a series of aromatic conjugated monoalkoxynaphthalene-naphthalimide donor-acceptor dyads is reported.
335x175mm (300 x 300 DPI)